

Optimizing standalone dual PV systems with four-port converter technology

Sharma Sha, Rajambal Kalayanasundaram

Department of Electrical and Electronics Engineering, Puducherry Technological University
(Erstwhile Pondicherry Engineering College), Puducherry, India

Article Info

Article history:

Received Mar 11, 2024

Revised Sep 9, 2024

Accepted Oct 23, 2024

Keywords:

DC-DC converter

Hybrid energy sources

Multiport converter

Photovoltaic system

PPAS control technique

ABSTRACT

This paper analyses the four-port converter (FPC) based PV system. The discussed FPC is developed for hybrid energy sources (HES) with the merits of a single converting stage, fewer switches, and simple topology. By tapping two source ports from the midway of its two switching legs, the FPC presented in this work is developed from the basic full bridge converter (FBC). The pulses are produced using the phase angle control with pulse width modulation (PPAS) technique. Different modes of operation of the FPC are analyzed elaborately to give an insight into its topology. To efficiently manage power distribution among the ports and regulate their voltage, two key control variables have been utilized: duty ratio and phase angle. An in-depth presentation is provided on the design and modeling of a four-port converter. It provides autonomous management of power allocation among terminals and regulation of load voltage. Finally, simulated key waveforms of the FPC and simulation results to demonstrate the decoupled regulation of power sharing and load voltage of a PV system under varying input and output conditions are presented. The experimental prototype of the four-port converter results is discussed and presented in detail.

This is an open access article under the [CC BY-SA](https://creativecommons.org/licenses/by-sa/4.0/) license.



Corresponding Author:

Sharma Sha

Department of Electrical and Electronics Engineering

Puducherry Technological University (Erstwhile Pondicherry Engineering College)

Puducherry, India

Email: sharmasha38@gmail.com, sharma.sha@ptuniv.edu.in

1. INTRODUCTION

Due to the continually increasing demand for energy, the world is attracted to renewable energy systems. Renewable energy sources (RES) can generate energy without affecting the environment, which is reproducible and can generate a tremendous amount of energy continuously. Enhancing the efficiency of the entire system is attainable via the integration of a photovoltaic (PV) system with an energy storage system (ESS). As illustrated in Figure 1, traditionally, different power sources are managed individually by multiple converters, each corresponding to the number of power sources cited in [1]-[5]. Figure 2 illustrates the range of multiport converters (MPCs) that have been created and planned to integrate numerous renewable energy systems and minimize the number of converters.

There are two types of multi-port converters, isolated topology and non-isolated topology mentioned in [6]. Multiport DC-DC converters with an isolated architecture are appropriate for high-voltage gain applications which use high-frequency transformers. However, the isolated transformer increases the size, cost, and losses. Low-voltage applications benefit more from non-isolated multiport DC-DC converters. Unidirectional converters are advised for their great efficiency and minimal switch count. The interface between the storage units is created via bidirectional converters. These are mentioned in several recent studies [7]-[12].

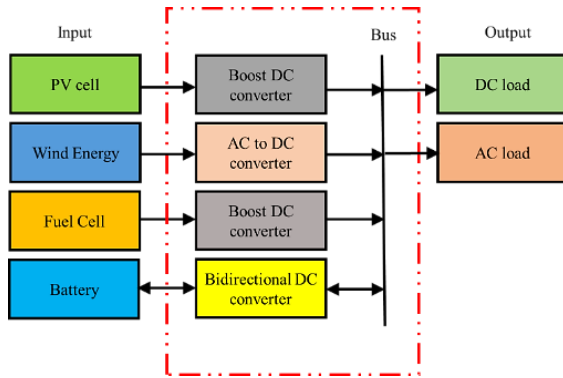


Figure 1. Integration of renewable energy sources with individual converters

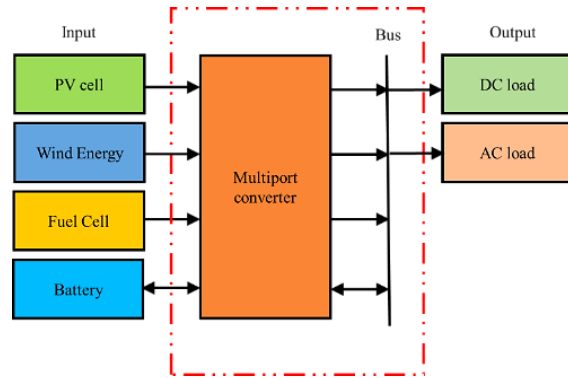


Figure 2. Sources with MPC

For standalone applications, a three-port converter is appropriate. For standalone systems, the renewable energy sources are linked to a three-port converter. Typically, the expansion of a three-port converter into a four-port converter involves the addition of one port to the system. The converters would be controlled by shifted-phase, interleaved switching signals with the same switching frequency. A simple boost converter raises a DC voltage by converting it. Reduced ripple currents in both the input and output circuits represent an additional benefit of interleaving. Sato *et al.* [13] say dividing the output current into two pathways results in higher efficiency and much lower I^2R and inductor alternating current (AC) losses. The interleaved boost converter stands out as an excellent option for high-power applications due to its ability to provide reduced input and output ripple, heightened efficiency, and increased power density. With an interleaved converter, you may get higher efficiency, lower ripple voltage, lower ripple inductor current, and faster switching speed mentioned in these articles [14]-[22].

In the pulse width modulation with phase angle shift (PPAS) control approach, the switch duty cycle and phase angle of interleaved converters serve as two independent control parameters shown in [23]. Liang *et al.* and Yadav *et al.* [24], [25] say that enables the attainment of decoupled voltage regulation across multiple ports within a specified operational range. Additionally, the phase angle adjustment of the interleaved buck-boost converter enhances control flexibility, facilitating precise management of secondary output voltage. By integrating ESS, one may achieve a broad output voltage gain, high efficiency, cheap cost, small size, and high stability about these techniques were analyzed in [26], [27].

This study focuses on a four-port converter comprising two photovoltaic (PV) inputs, a battery port, and a load port for analysis and get efficiency better than compared to the literatures. The converters are meticulously modeled and simulated using MATLAB/Simulink. The converter's performance is evaluated across different duty cycles, and the findings are comprehensively showcased. Furthermore, a hardware prototype of the four-port converter is developed to validate the simulation outcomes.

2. THE PROPOSED METHOD

The pulse width modulation (PWM) plus phase angle scheme for a four-port DC-DC converter enhances the control and efficiency of power distribution among multiple ports. In this scheme, each port can be independently controlled to optimize power transfer and minimize losses. PWM controls the duty cycle of the switching devices, regulating the average voltage, and current delivered to each port. By adjusting the pulse width, the converter can precisely manage the power flow to match the load requirements. Phase angle control adds another layer of precision by adjusting the timing of the switching devices within the converter. By setting the phase angles for each port, the scheme ensures that power transfer is not only efficient but also synchronized, reducing interference, and harmonics. This combined approach allows for the phase-shifted operation of multiple ports, which can help reduce the overall ripple and improve the dynamic response of the converter. Implementing this scheme in a four-port DC-DC converter involves a detailed control strategy. First, the phase angles for each port are calculated based on the load demands and the desired power sharing among the ports. These phase angles determine the timing of the switch activation. Next, PWM is applied within these phase-controlled periods to regulate the power delivered to each port. This synchronized approach ensures that the converter operates efficiently, providing stable and precise power to all connected loads. The PWM plus phase angle scheme is particularly beneficial in applications where multiple loads with different power requirements need to be managed simultaneously, such as in renewable energy systems, electric vehicles, and distributed power systems. It offers improved control, reduced electromagnetic

interference, and enhanced overall efficiency of the DC-DC conversion process. Figure 3 depicts the full bridge–four port converter (FB-FPC). It has two source ports that are linked to the PV array, as well as a storage port and a load port. The converter has two PV arrays are connected to the input port using a transformer with a turns ratio of 1: n. The primary side of the transformer employs a traditional full bridge converter, connecting two sources to the midpoint of each leg, thus establishing two-source ports. Moreover, a storage port is also integrated on the primary side. On the secondary side, a conventional diode bridge rectifier is employed, connected to the load port. When it is observed from the source port, the source port to the battery port forms a boost converter circuit. Hence as a whole primary side is composed of two PV ports, a battery port, and four switches to form a bi-phase boost converter or an interleaved boost converter.

As mentioned earlier, the input side of the converter under consideration features a full-bridge configuration, comprising complementary switches on each leg. Based on the duty ratio assigned to each leg, a rectangular voltage waveform is generated from the midpoint of each leg (U_a , U_b). The battery port is parallel-connected to the capacitor on the primary side to facilitate both charging and discharging operations. The power from the source like dual PV panels (Source port 1, Source port 2) is connected parallelly to each capacitor connected with inductors (L_1 , L_2). Switches S_1 , S_2 , S_3 , and S_4 constitute the complete bridge converter circuit. To regulate the power balance between the photovoltaic (PV) sources and the batteries, the duty ratio of switches S_1 and S_3 serves as two control variables (i.e D_{PV1} , D_{PV2}). The voltage difference between U_a and U_b , denoted as U_{ab} , is applied to the primary winding of the high-frequency transformer. Furthermore, the two voltages U_a and U_b are phase-shifted (ϕ), which is used as the third variable to control the output voltage.

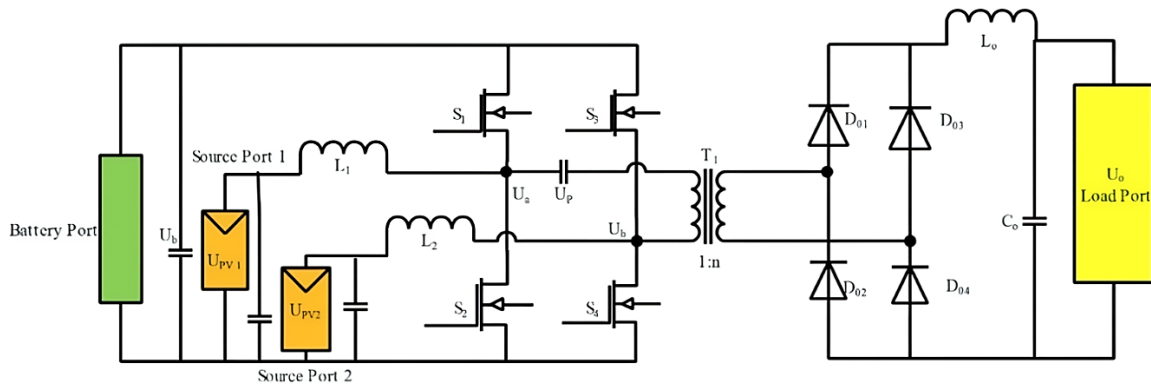


Figure 3. Full bridge four port converter

One switching cycle of period T_s comprises six states, as depicted in Figure 4. To produce a rectangular voltage from the midpoint of each leg, two switches on each leg operate in a complementary manner. The duty cycles of S_2 (S_1) and S_4 (S_3) function as a pair of control variables, governing the electrical power exchange among PV_1 and the energy storage unit, and PV_2 and the battery, correspondingly. Moreover, the two rectangular-waveform voltages, U_a and U_b , obtained from the midpoints of the two legs, are phase-shifted by an angle ϕ to control and regulate the output voltage U_o .

The transformer's turns ratio is denoted with a ratio of $N_p: N_s = 1: n$, with the voltage across the capacitor block C_b represented as U_{Cb} . Within one switching operations cycle, there are six switching states. Each state has corresponding equivalent circuit and switching table which is given in Figure 5 and Table 1 respectively. This state persists until S_1 is deactivated and S_2 is activated. Subsequently, a new switching period commences.

Table 1. Switching table

State	Switches ON	L1	L2	Diode ON	Primary voltage
I	S_2, S_3	Charges	Discharges	All	$-(U_b+U_{cb})$
II	S_2, S_3	Charges	Discharges	D_{01}, D_{04}	$-(U_b+U_{cb})$
III	S_2, S_4	Charges	Charges	D_{01}, D_{04}	$-U_{cb}$
IV	S_1, S_4	Discharges	Charges	All	U_b-U_{cb}
V	S_1, S_4	Discharges	Charges	D_{02}, D_{03}	U_b-U_{cb}
VI	S_1, S_3	Discharges	Discharges	D_{02}, D_{03}	$-U_{cb}$

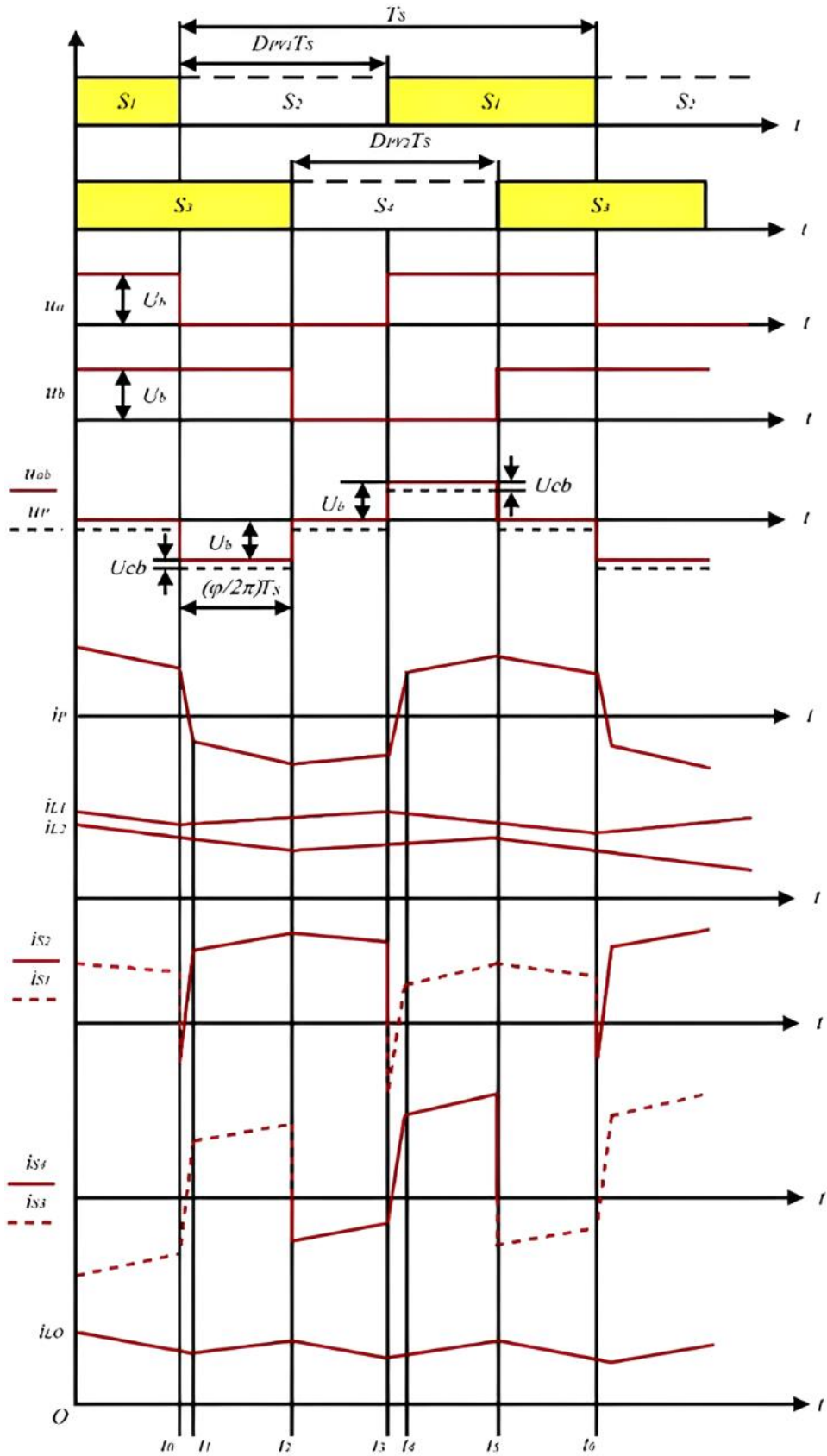


Figure 4. Switching modes of operation of FPC

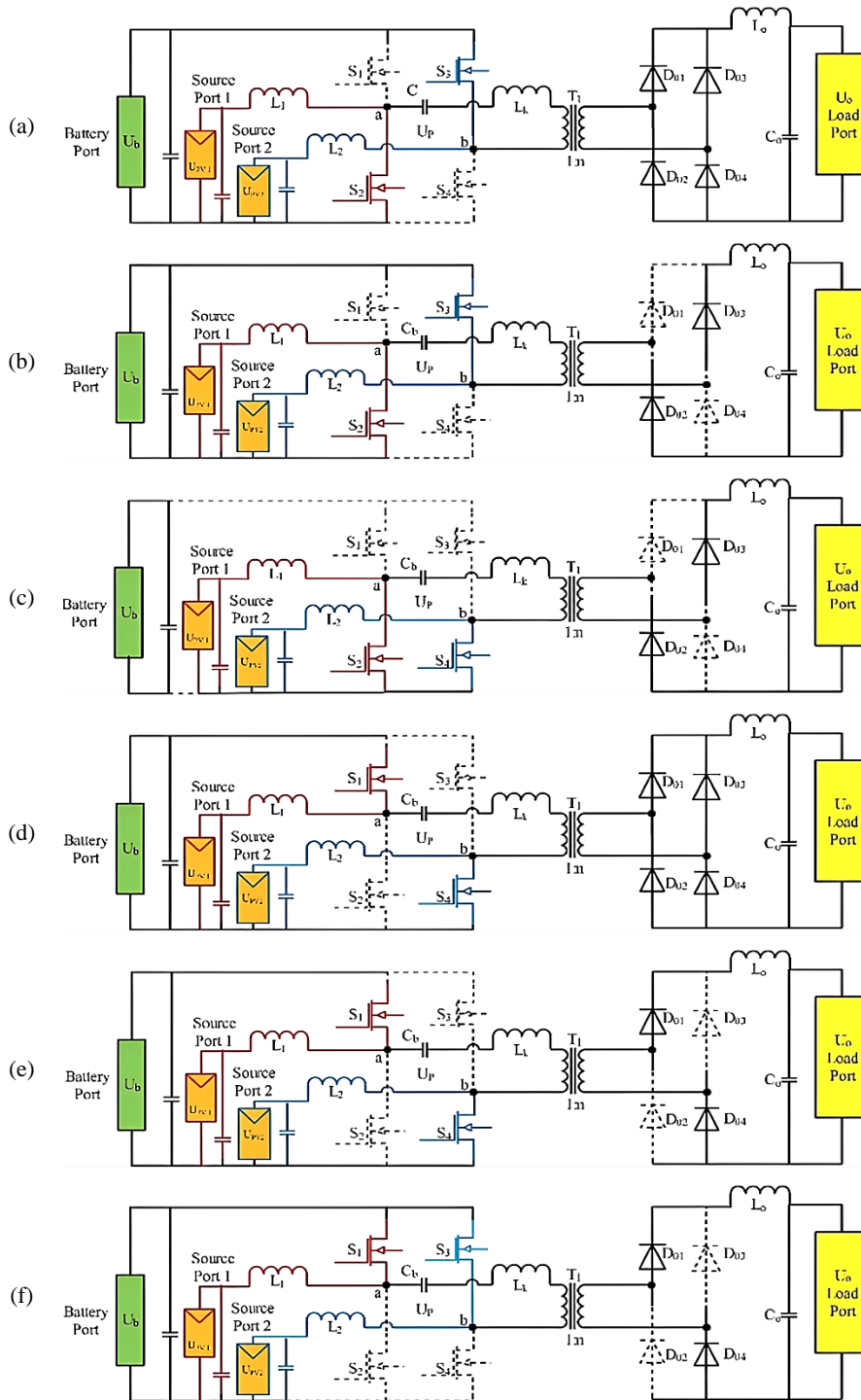


Figure 5. Equivalent circuit of FPC in different switching modes: (a) t_0-t_1 , (b) t_1-t_2 , (c) t_2-t_3 , (d) t_3-t_4 , (e) t_4-t_5 , and (f) t_5-t_6

The final output equation derived from the switching modes of the system written as (1).

$$U_o = \begin{cases} nU_b \left[\frac{\varphi}{2\pi} (1 - \Delta D_{PV21}) + 2\Delta D_{PV21} - 2\Delta D_{PV21}^2 \right], \Delta D_{PV21} > 0 \\ nU_b \left[\frac{\varphi}{2\pi} (1 + \Delta D_{PV21}) \right], \Delta D_{PV21} < 0 \\ nU_b \left[\frac{\varphi}{2\pi} \right], \Delta D_{PV21} = 0 \end{cases} \quad (1)$$

Where $\Delta D_{PV21} = D_{PV2} - D_{PV1}$. According to (1), the duty cycles D_{PV1} and D_{PV2} can be utilized to equalize the powers from the photovoltaic (PV) sources and the batteries, while the phase angle ϕ is adjustable to regulate the output voltage on the secondary side. These three control parameters ensure the full controllability of the four-variable system. Additionally, as illustrated in Figure 6, ensuring controllability of the phase angle ϕ involves a constraint. It can be written as (2). From Figure 6, it's evident that if the constraint condition isn't met, the output voltage U_o cannot be regulated solely by the phase angle ϕ . This situation leads to the loss of the control variable associated with the voltage output.

$$\frac{\phi}{2\pi} \leq D_{PV1} \text{ and } \frac{\phi}{2\pi} \leq 1 - D_{PV2} \quad (2)$$

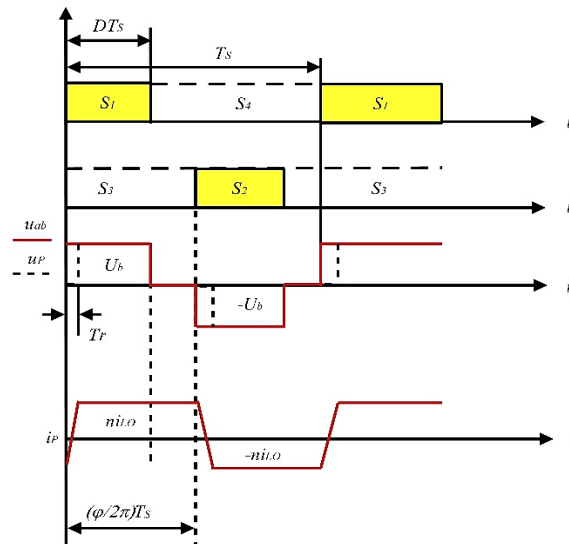


Figure 6. Primary voltage and current waveform for $\frac{\phi}{2\pi} \leq D, \frac{\phi}{2\pi} \leq (1 - D)$

3. SIMULATION RESULTS

The simulation model for the four-port converter is constructed using MATLAB/Simulink. Switching pulses are generated using a plus phase angle shift (PPAS) PWM scheme as discussed in section 2 with a switching frequency of 100 kHz. Table 2 gives the circuit parameters used for simulation. Two modules of Kyocera KD135GX-LP are connected in series to generate 270 W. A comprehensive analysis of the converter's performance is conducted, examining various solar irradiances and loading conditions in detail. The effect of duty ratio is studied and the results are discussed.

3.1. Simulation results for various solar irradiances

Figure 7 shows the simulation results at a rated irradiance of 1000 W/m² and duty ratio $D_{PV1} = D_{PV2} = 0.5$ with 0.25 phase shift. Figure 7(a) displays the switching pulses corresponding to switches S1-S4. The phase shift is noted to be 0.25. Figure 7(b) illustrates the resultant primary voltage and current, while Figure 7(c) depicts the resultant secondary voltage and current. The primary side inductor currents i_{L1} and i_{L2} are presented in Figure 7(d).

Simulation is carried out to study the performance of various solar irradiances. The irradiance is varied in steps and the results are observed and shown in Figure 8. As observed in Figures 8(a) and 8(b), the output voltage and current of the PV module demonstrate an increase with rising irradiance. The corresponding fluctuations in load voltage and current are observed and depicted in Figures 8(c) and 8(d) respectively. It is noted that the output voltage remains below the rated voltage of 100 V for irradiances below 700 W/m². Furthermore, the charging and discharging patterns of the battery under various irradiances are illustrated in Figures 8(e) and 8(f).

3.2. Effect of duty ratio and phase shift (ϕ)

The output voltage of the converter is controlled by adjusting the phase shift (ϕ). Figure 9 illustrates the variation of the phase shift with irradiance to maintain the output voltage at 100 V. It's observed that the phase angle decreases with an increase in irradiance to regulate the voltage. It is 0.25 at 1000 W/m² irradiance and increased progressively up to 0.35 for 400 W/m².

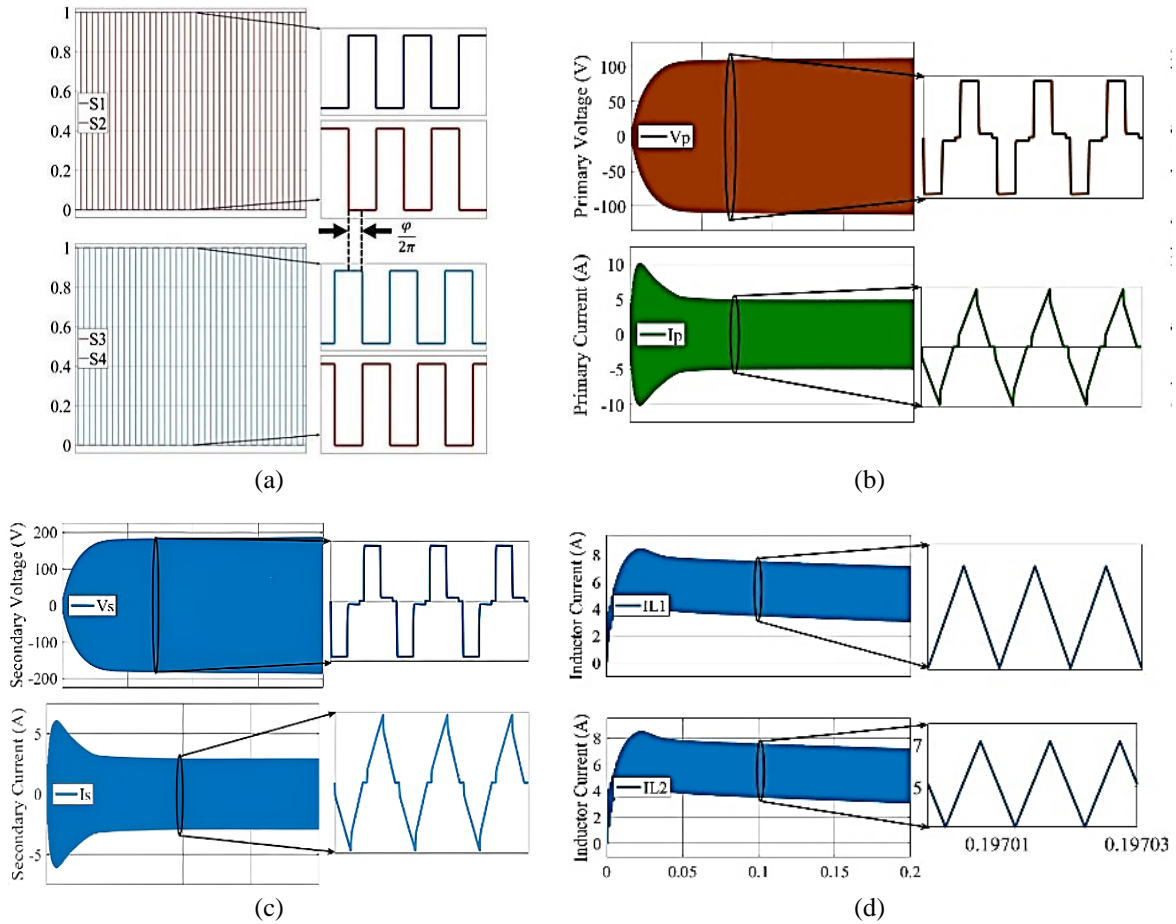


Figure 7. Simulation results at rated irradiance: (a) switching pulse of S₁-S₄, (b) primary side voltage and current, (c) secondary side voltage and current, and (d) inductor current of L₁ and L₂

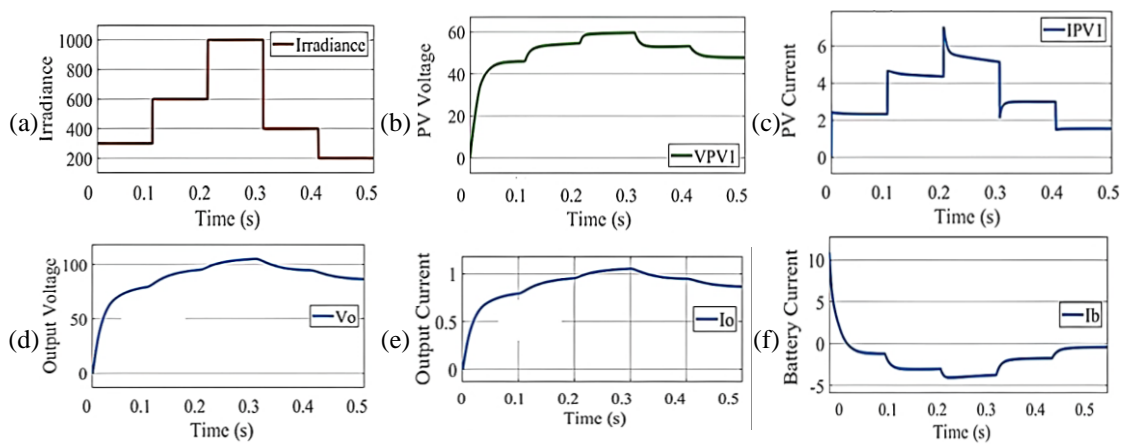


Figure 8. Simulation results of various solar irradiances: (a) various intensity, (b) PV voltage, (c) PV current, (d) output voltage, (e) output current, and (f) battery current

Table 2. Circuit parameters

Panel voltage (U_{pv1}, U_{pv2})	30 ~ 50 V	Panel voltage (U_{pv1}, U_{pv2})	30 ~ 50 V
Output voltage U_o	100 V	Output power (P_o)	0 ~ 500 W
Battery voltage U_b	75 V	Filter capacitors (C_o)	470 μ F
L_1 and L_2	72 μ H	Filter inductor (L_o)	80 μ H
Turns ratio (n)	1.66	Switching freq.	100 kHz
Panel power (P_{pv})	0 ~ 500 W		

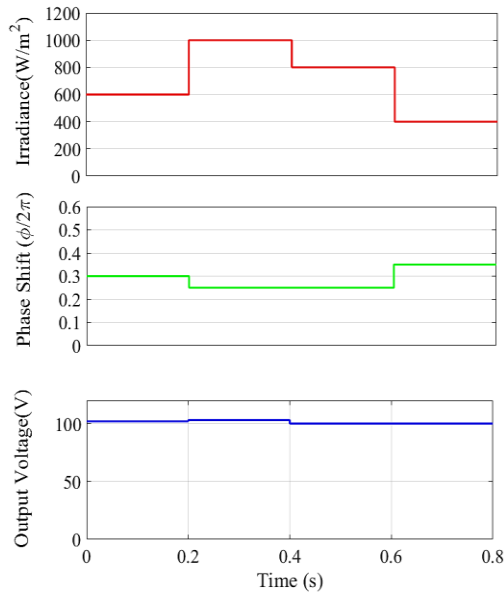


Figure 9. Output voltage regulation for various irradiances

4. CONCLUSION

A four-port converter, comprising a fundamental complete bridge and a bidirectional converter is analyzed. It delineates DC-linked sourcing/storage ports along with an isolated load port. The operational principles and diverse switching states are provided in the discussed topology. The utilization of pulse width modulation with phase angle shift facilitates decoupled management of power sharing and load voltage. Future work could focus on efficiency optimization, real-time implementation, and scalability to multi-port and renewable energy systems. Enhancements like fault tolerance, harmonic mitigation, and AI-based control can improve performance and adaptability. Additionally, an economic feasibility study can assess the topology's market potential.




REFERENCES

- [1] M. Rouhani and G. J. Kish, "Multiport DC–DC–AC modular multilevel converters for hybrid AC/DC power systems," *IEEE Transactions on Power Delivery*, vol. 35, no. 1, pp. 408–419, Feb. 2020, doi: 10.1109/TPWRD.2019.2927324.
- [2] J. Hong, J. Yin, Y. Liu, J. Peng, and H. Jiang, "Energy management and control strategy of photovoltaic/battery hybrid distributed power generation systems with an integrated three-port power converter," *IEEE Access*, vol. 7, pp. 82838–82847, 2019, doi: 10.1109/ACCESS.2019.2923458.
- [3] G. Zhang *et al.*, "A five-terminal impedance network based three-port converter," *IEEE Access*, vol. 6, pp. 29474–29485, 2018, doi: 10.1109/ACCESS.2018.2840528.
- [4] W. Kreeumporn and I. Ngamroo, "Optimal superconducting coil integrated into PV generators for smoothing power and regulating voltage in distribution system with PHEVs," *IEEE Transactions on Applied Superconductivity*, vol. 26, no. 7, pp. 1–5, Oct. 2016, doi: 10.1109/TASC.2016.2591981.
- [5] N. Saxena, I. Hussain, B. Singh, and A. L. Vyas, "Implementation of a grid-integrated PV-battery system for residential and electrical vehicle applications," *IEEE Transactions on Industrial Electronics*, vol. 65, no. 8, pp. 6592–6601, Aug. 2018, doi: 10.1109/TIE.2017.2739712.
- [6] S. A. Singh, G. Carli, N. A. Azeez, and S. S. Williamson, "Modeling, design, control, and implementation of a modified z-source integrated PV/Grid/EV DC charger/inverter," *IEEE Transactions on Industrial Electronics*, vol. 65, no. 6, pp. 5213–5220, Jun. 2018, doi: 10.1109/TIE.2017.2784396.
- [7] V. Monteiro, J. G. Pinto, and J. L. Afonso, "Experimental validation of a three-port integrated topology to interface electric vehicles and renewables with the electrical grid," *IEEE Transactions on Industrial Informatics*, vol. 14, no. 6, pp. 2364–2374, Jun. 2018, doi: 10.1109/TII.2018.2818174.
- [8] C. S. Goh, J. R. Kuan, J. H. Yeo, B. S. Teo, and A. Danner, "A fully solar-powered quadcopter able to achieve controlled flight out of the ground effect," *Progress in Photovoltaics: Research and Applications*, vol. 27, no. 10, pp. 869–878, Oct. 2019, doi: 10.1002/ppp.3169.
- [9] S. Moury and J. Lam, "A soft-switched, multiport photovoltaic power optimizer with integrated storage interface and output voltage regulation," *IEEE Transactions on Industrial Electronics*, vol. 68, no. 5, pp. 3917–3927, May 2021, doi: 10.1109/TIE.2020.2984432.
- [10] H. Zhang, D. Dong, M. Jing, W. Liu, and F. Zheng, "Topology derivation of multiple-port DC–DC converters based on voltage-type ports," *IEEE Transactions on Industrial Electronics*, vol. 69, no. 5, pp. 4742–4753, May 2022, doi: 10.1109/TIE.2021.3078389.
- [11] I. Askarian, M. Pahlevani, and A. M. Knight, "Three-port bidirectional DC/DC converter for DC nanogrids," *IEEE Transactions on Power Electronics*, vol. 36, no. 7, pp. 8000–8011, Jul. 2021, doi: 10.1109/TPEL.2020.3046453.
- [12] H. Nagata and M. Uno, "Nonisolated PWM three-port converter realizing reduced circuit volume for satellite electrical power systems," *IEEE Transactions on Aerospace and Electronic Systems*, vol. 56, no. 5, pp. 3394–3408, Oct. 2020, doi: 10.1109/TAES.2020.2971287.
- [13] Y. Sato, M. Uno, and H. Nagata, "Nonisolated multiport converters based on integration of PWM converter and phase-shift-switched capacitor converter," *IEEE Transactions on Power Electronics*, vol. 35, no. 1, pp. 455–470, Jan. 2020, doi: 10.1109/TPEL.2019.2912550.




- [14] Y. Sato, H. Nagata, and M. Uno, "Nonisolated single-magnetic multi-port converter based on integration of PWM converter and dual active bridge converter," in *2018 IEEE 18th International Power Electronics and Motion Control Conference (PEMC)*, IEEE, Aug. 2018, pp. 157–163, doi: 10.1109/EPEPEMC.2018.8521879.
- [15] H. Yang, S. Luo, X. Sun, Q. Zhang, and Y. Zhong, "Research on adrc method for bidirectional DC-DC converter of solar energy storage system," *Acta Energiæ Solaris Sinica*, vol. 39, no. 5, pp. 1342–1350, 2018.
- [16] Y. Sato, H. Nagata, and M. Uno, "Non-isolated multi-port converter integrating PWM and phase-shift converters," in *TENCON 2017 - 2017 IEEE Region 10 Conference*, IEEE, Nov. 2017, pp. 1097–1102, doi: 10.1109/TENCON.2017.8228021.
- [17] A. K. Bhattacharjee and I. Batarseh, "An interleaved boost and dual active bridge-based single-stage three-port DC-DC-AC converter with sine PWM modulation," *IEEE Transactions on Industrial Electronics*, vol. 68, no. 6, pp. 4790–4800, Jun. 2021, doi: 10.1109/TIE.2020.2992956.
- [18] J. Zeng, J. Ning, X. Du, T. Kim, Z. Yang, and V. Winstead, "A four-port DC-DC converter for a standalone wind and solar energy system," *IEEE Transactions on Industry Applications*, vol. 56, no. 1, pp. 446–454, 2019, doi: 10.1109/TIA.2019.2948125.
- [19] H. Wu, P. Xu, H. Hu, Z. Zhou, and Y. Xing, "Multiport converters based on integration of full-bridge and bidirectional DC-DC topologies for renewable generation systems," *IEEE Transactions on Industrial Electronics*, vol. 61, no. 2, pp. 856–869, Feb. 2014, doi: 10.1109/TIE.2013.2254096.
- [20] P. Prabhakaran and V. Agarwal, "Novel four-port DC-DC converter for interfacing solar PV-fuel cell hybrid sources with low-voltage bipolar DC microgrids," *IEEE Journal of Emerging and Selected Topics in Power Electronics*, vol. 8, no. 2, pp. 1330–1340, Jun. 2020, doi: 10.1109/JESTPE.2018.2885613.
- [21] Q. Tian, G. Zhou, M. Leng, G. Xu, and X. Fan, "A nonisolated symmetric bipolar output four-port converter interfacing PV-battery system," *IEEE Transactions on Power Electronics*, vol. 35, no. 11, pp. 11731–11744, Nov. 2020, doi: 10.1109/TPEL.2020.2983113.
- [22] T. Chaudhury and D. Kastha, "A high gain multiport DC-DC converter for integrating energy storage devices to DC microgrid," *IEEE Transactions on Power Electronics*, vol. 35, no. 10, pp. 10501–10514, Oct. 2020, doi: 10.1109/TPEL.2020.2977909.
- [23] P. Kolahian, H. Tarzami, A. Nikafrooz, and M. Hamzeh, "Multi-port DC-DC converter for bipolar medium voltage DC micro-grid applications," *IET Power Electronics*, vol. 12, no. 7, pp. 1841–1849, Jun. 2019, doi: 10.1049/iet-pel.2018.6031.
- [24] Y. Liang, H. Zhang, M. Du, and K. Sun, "Parallel coordination control of multi-port DC-DC converter for stand-alone photovoltaic-energy storage systems," *CPSS Transactions on Power Electronics and Applications*, vol. 5, no. 3, pp. 235–241, Sep. 2020, doi: 10.24295/CPSSPEA.2020.00020.
- [25] S. K. Yadav, N. Mishra, and B. Singh, "Multilevel converter with nearest level control for integrating solar photovoltaic system," *IEEE Transactions on Industry Applications*, vol. 58, no. 4, pp. 5117–5126, Jul. 2022, doi: 10.1109/TIA.2022.3177399.
- [26] Z. Lin, S. Pan, Y. Chen, W. Lin, J. Gong, and X. Zha, "A dual-input mismatch power processing LLC converter for microinverter application," *IEEE Transactions on Industrial Electronics*, vol. 71, no. 10, pp. 12487–12498, Oct. 2024, doi: 10.1109/TIE.2024.3355513.
- [27] R. Chakraborty and O. Ray, "Analysis of direct-duty-ratio based MPPT control scheme for integrated dual-DC boost converter," in *2022 IEEE Energy Conversion Congress and Exposition (ECCE)*, IEEE, Oct. 2022, pp. 1–6, doi: 10.1109/ECCE50734.2022.9948190.

BIOGRAPHIES OF AUTHORS



Sharma Sha    received his bachelor of technology degree in electrical and electronics engineering from Pondicherry University in the year 2016. He completed a masters of technology degree in renewable energy from Gandhigram Rural Institute in the year 2019. Currently, he pursuing Ph.D. degree from Puducherry Technological University (Erstwhile Pondicherry Engineering College). His areas of research expand power electronics, renewable energy systems, and electrical machines. He can be contacted at email: sharmasha38@gmail.com or sharma.sha@ptuniv.edu.in.



Rajambal Kalayanasundaram    received her bachelor of engineering degree in electrical engineering and master of engineering degree in power electronics from Anna University, Chennai, India, in 1991 and 1993, respectively. She received her Ph.D. degree in electrical engineering from Anna University in 2005. Currently, she is working as a professor in the Electrical and Electronics Engineering Department of EEE at Puducherry Technological University (Erstwhile Pondicherry Engineering College). Her areas of research include power electronics, electrical drives, renewable energy systems, and electric vehicles. She can be contacted at email: rajambalk@ptuniv.edu.in.